applied sciences

MDPI

Article

Comments on the Physics of Microwave-Undulators

Emanuele Di Palma [1,*,†], Giuseppe Dattoli [1,†] and Svilen Sabchevski [2,†]

[1] ENEA—Frascati Research Center, Via Enrico Fermi 45, 00044 Rome, Italy
[2] Institute of Electronics of the Bulgarian Academy of Sciences, 1784 Sofia, Bulgaria
* Correspondence: emanuele.dipalma@enea.it; Tel.: +39-06-9400-5709
† These authors contributed equally to this work.

Abstract: The properties of electromagnetic undulators, produced by the field of a high-power microwave, are discussed. We analyze the conditions to be satisfied that allow the treatment of the emission process by relativistic charges moving through it in full analogy with the case of their static counterparts. We critically review the often claimed possibility of exploiting them in programs aimed at reducing the sizes and costs of an actual free electron laser (FEL) device. We analyze several possible configurations for FELs based on powerful microwave undulators and conclude that the present level of technology, even though not yet mature, should be improved to allow a breakthrough either for low- or high-gain devices.

Keywords: RF wave undulator; free electron laser; linac; synchrotron radiation; beam transport optics

Citation: Di Palma, E.; Dattoli, G.; Sabchevski, S. Comments on the Physics of Microwave-Undulators. *Appl. Sci.* **2022**, *12*, 10297. https://doi.org/10.3390/app122010297

Academic Editor: Bernhard Wilhelm Roth

Received: 24 August 2022
Accepted: 4 October 2022
Published: 13 October 2022

1. Introduction

The electromagnetic field constrained in a waveguide can impress an oscillatory motion to an electron (or to an electron beam) moving through it. The action is therefore not dissimilar from the role played by the static field of a magnetic undulator, constituting the core of any Free Electron Laser (FEL) device.

Accordingly, the high power of microwave fields passing through a waveguide could provide the essential tool for the realization of Wave Undulator (WU) based FELs. Although the concept is by no means new and traces back to the 1980s (see [1–18] for an albeit partial list), the development of high powerC/X-band sources (and not only) for high gradient accelerators [10] could provide the technologies necessary for an effective development of WU-FELs. The advantages offered by this solution are evident in terms of radiation polarization, effect of wake field mitigation on the beam itself (with the consequent possibility of operating with larger currents), and reduction of costs and physical size.

The disadvantages are easily summarized by observing that in spite of the claimed perspective superiority with respect to the its magnetic counterpart and in spite of the fact that the relevant proposals are more than forty years old, no WU-FEL has been operated so far.

The spontaneous radiation from an S-Band wave and electron beam with energy above 100 MeV has been experimentally studied in ref. [5]. This paper had many merits and revealed many interesting features, the first of which is that of putting in clear evidence that, by using the adequate correspondences, the magnetic and WU bremsstrahlung processes can be treated on the same ground.

This aspect of the problem was initially studied in [6], and in ref. [11], a proposal has been put forward for the construction of a short wavelength FEL operating with an X-Band WU.

In more recent times, the problem has been further studied and different types of WU have been proposed, along with various types of FEL architectures, including laser wave undulators as well (see [19] and reference therein).

Even though we have not specified what the drawbacks of a WU-FEL are, it is evident that most of the problems arise from the large amount of microwave power necessary to feed the cavity to reach a reasonable strength parameter from the mechanical machining of the waveguide itself and from the power attenuation along the propagation. All these effects cause inhomogeneous broadening, which combine with the other well-known emission line degrading effects, thus inducing further potentially harmful contributions degrading the FEL gain and its performances.

In this paper, we take advantages from the previously quoted studies to propose a comprehensive and accurate investigation of the microwave–electron interaction mechanisms to address a more appropriate direction to the strategies developed for the design of FELs operating with microwave undulators. In the past, the problem has been treated using a rather pragmatic point of view. Most of the treatment has been that of "viewing" the microwave field as static, thus associating to it an equivalent period, a peak magnetic field and, accordingly, an equivalent strength parameter. This procedure is in some sense the inverse of the Weiszacker–Williams approximation (WW-A) [20] exploited by Madey in his seminal paper [21] to treat the emission process by relativistic electron in undulators as a scattering process of the undulator associated virtual photons [22–24].

The reverse point of view is, in principle, legitimate. It should be, however, properly framed within the context of an accurate understanding of the equations modeling the spectral details of the radiation emitted by relativistic electrons propagating in a microwave undulator.

Before entering the core of the discussion developed in the forthcoming sections, we summarize the points we will carefully treat in the following.

The paradigmatic assumptions underlying the hypothesis of an inverse WW-A are the definition of the microwave undulator (MU) equivalent period λ_u and magnetic field B_u. As we will see in the following, they should be respectively specified as (see ref. [5,10] and the forthcoming sections for the appropriate mathematical analysis)

$$\begin{aligned} \lambda_u &= \frac{\lambda}{1+\sqrt{1-\left(\frac{\omega_c}{\omega}\right)^2}}, \\ B_u &= \frac{E_0}{c}\left(1+\sqrt{1-\left(\frac{\omega_c}{\omega}\right)^2}\right), \end{aligned} \tag{1}$$

where E_0 is the intensity of the microwave peak electric field, $\omega_c = \pi c/a$ is the cutoff frequency, with a the waveguide dimension (see Figure 1), c is the speed of light, and ω and λ are the operating angular frequency and wavelength, respectively.

Accordingly we can define the corresponding K-strength as [25]

$$K_u = \frac{eB_u\lambda_u}{2\pi m_e c} = \frac{e\,E_0\lambda}{2\,\pi\,m_e c^2}, \tag{2}$$

with m_e being the electron mass.

It's worth noting that, from Equation (2), the relation between the electric field peak intensity of the microwave and the associated K value is given by

$$E[V/m] \sim \sqrt{3}10^{-3}\omega[Hz]K. \tag{3}$$

Assuming $\lambda/\lambda_u = 2$ and using the parameters of the European X-FEL [26] undulators, we derive from Equation (3) a peak electric field around 300 MV/m, which is hard to manage in a microwave waveguide. Accordingly, ω being fixed by the waveguide geometrical constraints, the only way to reduce the peak electric field value is to operate at lower K values.

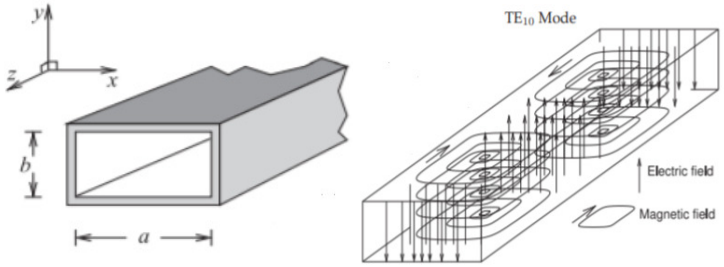

Figure 1. Three-dimensional view of a waveguide (on the **left**). Electromagnetic field distribution for the mode TE_{01} (on the **right**).

Together, Equations (1)–(3) offer the key relations for a quick design of an MU dedicated to FEL operation [10]. These elements, however, are not sufficient to avoid design and conceptual pitfalls.

For example, a problem of not secondary importance, such as the evaluation of the detrimental effects of the microwave field inhomogeneities, has been only superficially included in the MU-FEL design.

This paper is aimed at filling a gap. Even though undulators based on the use of electromagnetic waves for FEL operation are often "invoked", a thorough analysis of how the design parameters should be embedded is still lacking.

Therefore, a more adequate approach is necessary to stay on the safe side. In the forthcoming sections, we address the following points:

(a) Write and integrate the equation of motion of electrons in the MU-field.
(b) Discuss the properties of the radiation emitted by relativistic electrons moving inside the microwave.
(c) Specify the conditions under which the MU can be exploited to drive an FEL either in the oscillator or SASE configuration. We will, in particular, discuss how the inhomogeneities associated with the electron–MU interaction should be included to evaluate the gain reduction effects and state the limits of safe operation.

2. Microwave Field Equation

To begin with, we consider a simple but insightful example of a rectangular waveguide in which a $TE_{0,1}$ mode is excited with side orientation reported in Figure 1.

In such a configuration, the electromagnetic field components write [5,10]

$$\begin{aligned} E_x &= E_0 \sin\left(\frac{\pi y}{a}\right) \sin(\omega t + k_g z), \\ B_y &= \frac{E_0}{c} \sin\left(\frac{\pi y}{a}\right) \sqrt{1 - \left(\frac{\omega_c}{\omega}\right)^2} \sin(\omega t + k_g z), \\ B_z &= \frac{E_0}{c} \cos\left(\frac{\pi y}{a}\right) \frac{\omega}{\omega_c} \cos(\omega t + k_g z), \\ k_g &= \frac{\omega}{c} \sqrt{1 - \left(\frac{\omega_c}{\omega}\right)^2}, \\ \omega_c &= \frac{\pi c}{a}. \end{aligned} \tag{4}$$

In Figure 1, we have also reported the field line distribution along the waveguide for completeness sake. The motion of a relativistic electron along the waveguide is ruled by the Lorentz force

$$m \frac{d(\gamma \dot{\vec{r}})}{dt} = -e\vec{E} - e\vec{v} \times \vec{B}, \tag{5}$$

where $\vec{r}$ is the particle position, and γ is the electron relativistic factor. The previous vector differential equation can be cast in the following explicit form:

$$\begin{aligned}
&m_e\gamma\frac{d\beta_x}{dt}+m_e\beta_x\frac{d\gamma}{dt}=-\frac{eE_0}{c}\sin\left(\frac{\pi y}{a}\right)\left[1+\frac{\omega_g}{\omega}\beta_z\right]\sin(\omega t+k_g z)\\
&-\frac{eE_0}{c}\beta_y\cos\left(\frac{\pi y}{a}\right)\frac{\omega_c}{\omega}\cos(\omega t+k_g z),\\
&m_e\gamma\frac{d\beta_y}{dt}+m_e\beta_y\frac{d\gamma}{dt}=-e\frac{E_0}{c}\beta_x\cos\left(\frac{\pi y}{a}\right)\frac{\omega_c}{\omega}\cos(\omega t+k_g z),\\
&m_e\gamma\frac{d\beta_z}{dt}+m_e\beta_z\frac{d\gamma}{dt}=e\frac{E_0}{c}\frac{\omega_g}{\omega_c}\beta_x\sin\left(\frac{\pi y}{a}\right)\sin(\omega t+k_g z),\\
&m_e c^2\frac{d\gamma}{dt}=-e\vec{E_0}\cdot\vec{v},
\end{aligned}\tag{6}$$

where $\beta_{x,y,z}$ is the electron velocity along the coordinates axes normalized to c, and $\omega_g=2\pi c/\lambda_g$, where $\lambda_g=2\pi/k_g$ is the guide wavelength.

Confronting the physics underlying the previous equations with those regarding the motion of electrons in a static undulator field, we can note that the combined presence of electric and magnetic fields does not allow the conservation of the total velocity. Furthermore, the equations are explicitly time-dependent.

As also noted in ref. [10], the dynamics of electrons ruled by Equation (6) are associated with the transverse electric and magnetic fields and by the longitudinal magnetic component.

The first produces the ordinary wiggling motion. On the other side, the longitudinal magnetic field and the wiggling is responsible for a nonlinear defocusing force, commented on in the following.

We can simplify Equation (6) by means of the assumption that the velocity squared remains almost unchanged and that it points essentially along the longitudinal direction, which implies that the energy is practically conserved, namely that in Equation (6) $\frac{d\gamma}{dt}\cong 0$.

According to this assumption, we set $t\cong\frac{z}{c}$, and the argument of the oscillating functions becomes:

$$\begin{aligned}
&(\omega t+k_g z)\cong(k+k_g)\,z,\\
&\omega=\frac{2\pi\,c}{\lambda}.
\end{aligned}\tag{7}$$

Furthermore, writing $k_u=k+k_g$, we find

$$\frac{2\pi}{\lambda_u}=\frac{2\pi}{\lambda}+\frac{2\pi}{\lambda_g},\tag{8}$$

which justifies the first of Equation (1).

We can integrate Equation (6) assuming ultra-relativistic electron motion and keeping contributions at the lowest order in $1/\gamma$; therefore setting $y\cong y_0$ and $\beta_z\cong 1$, we find for the x-component

$$\begin{aligned}
&\frac{d\beta_x}{dt}=-A\sin(\omega_u t)-B\cos(\omega_u t),\\
&A=\frac{eE_0}{m\gamma c}\sin\left(\frac{\pi\,y_0}{a}\right)\left[1+\frac{\omega_g}{\omega}\right],\\
&B=\frac{eE_0}{m\gamma\,c}\cos\left(\frac{\pi\,y_0}{a}\right)\frac{\omega_c}{\omega},
\end{aligned}\tag{9}$$

which, once integrated, eventually yields

$$\beta_x(t) = \beta_x^0 - \frac{A}{\omega_u}(1 - \cos(\omega_u t)) - \frac{B}{\omega_u}\sin(\omega_u t), \tag{10}$$

for the reduced velocity and

$$x(t) = v_x^0 t - \frac{Ac}{\omega_u}\left(t - \frac{1}{\omega_u}\sin(\omega_u t)\right) - \frac{Bc}{\omega_u^2}(1 - \cos(\omega_u t)), \tag{11}$$

for the position.

The equation ruling the y-component is obtained by the use of the same procedure. and indeed we obtain

$$\begin{aligned} \frac{d\beta_y}{dt} &= -C\beta_x \cos(\omega_u t), \\ C &= e\frac{E_0}{m\gamma c}\cos\left(\frac{\pi y_0}{a}\right)\frac{\omega_c}{\omega}. \end{aligned} \tag{12}$$

Inserting (9) in the previous equation, we are left with

$$\begin{aligned} \frac{d\beta_y}{dt} &= -C\cos(\omega_u t)\left[\beta_x^0 - \frac{A}{\omega_u}(1 - \cos(\omega_u t)) - \frac{B}{\omega_u}\sin(\omega_u t)\right] = \\ &= -C\left(\beta_x^0 - \frac{A}{\omega_u}\right)\cos(\omega_u t) - \frac{AC}{\omega_u}\cos(\omega_u t)^2 + \frac{BC}{\omega_u}\cos(\omega_u t)\sin(\omega_u t) = \\ &= -\frac{AC}{2\omega_u} - C\left(\beta_x^0 - \frac{A}{\omega_u}\right)\cos(\omega_u t) - \frac{C}{2\omega_u}(A\cos(2\omega_u t) - B\sin(2\omega_u t)) \end{aligned} \tag{13}$$

and, limiting ourselves to the integration of the non-oscillating part only, we obtain

$$\beta_y = \beta_y^0 - \frac{AC}{2\omega_u}t, \tag{14}$$

and

$$y = v_y^0 t - \frac{AC}{8\pi}\lambda_u t^2. \tag{15}$$

Thus, the motion along the y-direction is accordingly characterized by a parabolic drift.

We have checked the consistency of our approximation by a full integration of Equation (6) and a comparison with the analytical treatment.

In Figure 2 we have reported the behavior of the energy vs. time and the x,y-trajectories for the case of the parameters reported in the captions. The particles are injected around the center of a waveguide with sides X = 2.5 cm, Y = 5 cm.

The energy is essentially conserved, and the transverse dynamics reflect the superposition of different oscillating components

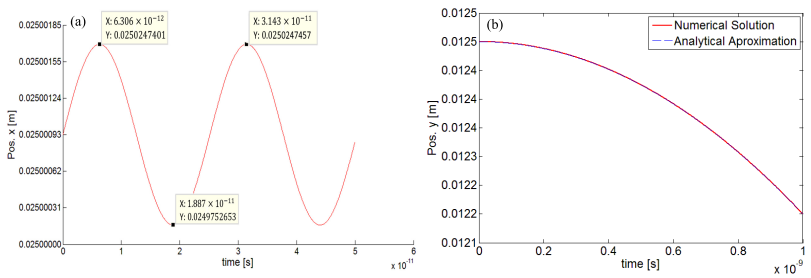

Figure 2. (**a**) Comparison between numerical and analytical solution for the x-motion component; (**b**) same as (**a**) for the y-position (simulation parameters).

It is evident that the comparison between analytical and numerical solutions is excellent; however, the injection at the point we have specified is not useful for our purposes. The electron trajectory undergoes significant deviations in the transverse directions which, if not properly corrected, may cause the loss of the beam itself.

We therefore consider the particle injection in such a way that (initially) $\frac{\pi y_0}{a} \cong \frac{\pi}{2}$. Under such a condition, the magnetic field component along the $z-$*direction* is initially vanishing and remains such if the y component has no significant drift during the particle transit inside the waveguide.

Equation (6) eventually reduces to

$$\begin{aligned} m_e\gamma\frac{d\beta_x}{dt} &= -\frac{eE_0}{c}\left[1+\frac{\omega_g}{\omega}\right]\sin(k_u z), \\ m_e\gamma\frac{d\beta_y}{dt} &= 0, \\ m_e\gamma\frac{d\beta_z}{dt} &= e\frac{E_0}{c}\frac{\omega_g}{\omega_c}\beta_x\sin(k_u z). \end{aligned} \tag{16}$$

By further pushing our approximations, we can write the first of Equation (9) as

$$\ddot{x} = -c\frac{K_u k_u}{\gamma}\dot{z}\sin(k_u z). \tag{17}$$

In conclusion, the results we have obtained are indeed consistent with the integration of the equations of motion of a (ultra)-relativistic electron moving in a magnetostatic undulator, whose vector field distribution is

$$\vec{B} \equiv (0, B_u\sin(k_u z), 0), \tag{18}$$

provided that the equivalent magnetic field and period be those given, respectively, in the second and first of Equation (1). The integration of Equation (17) at the lowest order in K_u/γ (or simply specializing Equations (9), (14) and (15)), yields

$$\dot{x}(t) = \dot{x}_0 - \frac{cK_u}{\gamma}(1-\cos(\omega_u t)). \tag{19}$$

After a further integration, we find

$$\begin{aligned} x(t) &= \dot{x}_0 t - \frac{cK_u}{\gamma}\left(t - \frac{1}{\omega_u}\cos(\omega_u t)\right) = \left(\dot{x}_0 - \frac{cK_u}{\gamma}\right) + A\cos(\omega_u t), \\ A &= \frac{cK_u}{\gamma\omega_u} = \frac{K_u}{\gamma}\frac{\lambda_u}{2\pi}. \end{aligned} \tag{20}$$

Finally, the longitudinal dynamics are governed by the (approximate) conservation of the velocity, which yields

$$\dot{z}(t)^2 = c^2\left(1 - \frac{K_u^2}{\gamma^2}\cos(\omega_u t)^2\right). \tag{21}$$

It can be integrated straightforwardly, and in the ultra-relativistic limit we find

$$\begin{aligned} z &\cong \bar{v}_z t - \frac{\pi A^2}{8\lambda_u}\sin(2\omega_u t), \\ \bar{v}_z &= \left(1 - \frac{1}{2\gamma^2}\left(1+\frac{K_u^2}{2}\right)\right)c, \end{aligned} \tag{22}$$

where $\bar{v}_z$ is the average velocity of electrons along the z-direction. In a reference frame moving with this velocity, we obtain, for x, z the trajectories the equations of motion (primed quantities label the dynamics in the moving frame) (for further details see [24])

$$x'(t') = x(t) = A\cos(\omega' t'),$$
$$z'(t') = \frac{A}{8}\frac{K_u}{\sqrt{1+\frac{K_u^2}{2}}}\sin(2\omega' t'), \tag{23}$$

with

$$t' = \frac{t}{\gamma} \text{ and } \omega' = \gamma\omega_u = \frac{1}{\sqrt{1+\frac{K_u^2}{2}}}\left(1+\sqrt{1-\left(\frac{\omega_c}{\omega}\right)^2},\right)\omega \tag{24}$$

Equation (23) is the parametric representation of the lemniscates, namely the 8-like motion ensuring the departure of the electron motion from the ordinary dipole oscillations.

In Figure 3, we have benchmarked the correctness of the analytical computations against the numerical integration. The comparison confirms the correctness of our approximations.

In particular, we have checked that the amplitude of the oscillations are those predicted by Equation (20); hence the definition of the equivalent strength parameter given in Equation (2) sounds reliable. The oscillation period is in perfect agreement with the introduction of the equivalent undulator period in Equation (1).

We have underscored these well-known issues because these are the distinctive features leading to the peculiar radiation emission inside linearly polarized magnetic undulators. In particular, the lemniscate-like motion (see Figure 3b) is a signature of the nondipolar nature of the electron motion and, accordingly, the emission pattern of the radiation inside the waveguide is not simply associated with the conventional antenna radiation mechanism, and we may expect higher odd-harmonics on axis emission.

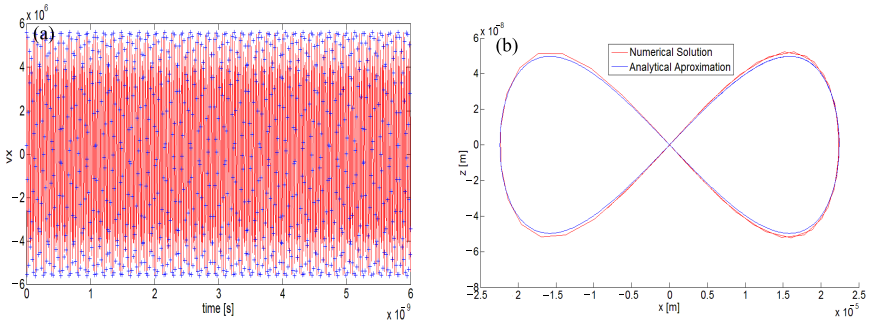

Figure 3. (**a**) X-component electron velocity (numerical red, blue crosses analytical); (**b**) eight-like motion in the laboratory frame (blue analytical, red numerical). We have plotted indeed $z - \bar{v}_z t$ vs. x both evaluated in the laboratory frame.

In the forthcoming section, we will discuss the consequences of the previous considerations for the design of MU-based FEL devices.

3. MU Spectral Properties and Low Gain FEL Devices

According to our previous results, we may safely conclude that the spectrum of the radiation emitted by the electrons traversing the waveguide is fully consistent with that from electrons moving in a conventional undulator (with a periodic static magnetic field).

The spectrum consists of a series of peaks centered at the wavelength provided by (n is the order of the harmonics)

$$\begin{aligned} \lambda_{r,n} &= \frac{\lambda_r}{n}, \\ \lambda_r &= \frac{\lambda_u}{2\gamma^2}\left(1+\frac{K_u^2}{2}+(\gamma\vartheta)^2\right), \end{aligned} \tag{25}$$

where ϑ is the observation angle.

The power radiated inside the waveguide and the relevant spectral details can be obtained using standard means. By just applying the ordinary tools [25,27,28] and neglecting the contributions due to higher harmonics, we find that the power emitted per unit solid angle in the forward direction by a single electron is

$$\begin{aligned} &\frac{dP}{d\Omega} \cong \dot{N}_\Omega \hbar \omega_{r,1}\ , \\ &\dot{N}_\Omega = \frac{\alpha K_u^2}{4\pi}\frac{\omega_r}{1+\frac{K_u^2}{2}}, \\ &\omega_{r,1} = \frac{2\pi c}{\lambda_r}, \lambda_r = \frac{\lambda_u}{2\gamma^2}\left(1+\frac{K_u^2}{2}\right), \\ &\alpha = \frac{1}{4\pi\,\varepsilon_0}\frac{e^2}{\hbar c}, \end{aligned} \tag{26}$$

where $\dot{N}_\Omega$ denotes the number of photons emitted per unit time and unit solid angle. The presence of the Planck constant is artificial; the process is indeed purely classical.

The power integrated on the whole solid angle in terms of the waveguide parameters reads

$$\begin{aligned} P_1 &\cong \frac{\pi}{3} N_u \dot{N}_\Omega \frac{I}{I_A} m_e c^2, \\ N_u &= \frac{L\lambda}{\lambda_u}, \end{aligned} \tag{27}$$

where N_u is the number of periods associated with the MU, and I, I_A are the beam and Alfvèn current, respectively.

In the previous formula, we neglected the effects of the lemniscates type motion due to the nondipolar longitudinal oscillations. The inclusion of the associated contributions provides the emission of all harmonics all over the solid angle and one obtains (for a single electron)

$$\begin{aligned} P_{sy} &= \frac{1}{12\pi^2}\alpha\hbar\frac{\omega_{sy}^2}{\left(1+\sqrt{1-\left(\frac{\omega_c}{\omega}\right)^2}\right)^2}, \\ \omega_{sy} &= 2\pi\gamma\frac{eE_0\left(1+\sqrt{1-\left(\frac{\omega_c}{\omega}\right)^2}\right)}{m\,c}. \end{aligned} \tag{28}$$

The previous result is interesting (albeit a natural consequence of the analysis developed so far) because it states that the total emitted power in the waveguide is equivalent to that radiated in a bending magnet with the equivalent magnetic field provided by B_u in Equation (1).

The radiation emitted at odd harmonics (at $\vartheta = 0$) per unit solid angle and unit frequency is specified by

$$\begin{aligned}
&\frac{d^2I}{d\Omega d\omega} = A_n(\omega)F_n(K_u),\\
&A_n(\omega) \propto \left[\frac{\sin\left(\frac{\nu_n}{2}\right)}{\frac{\nu_n}{2}}\right]^2,\ \nu_n = 2\pi N_u\left(\frac{\omega - n\omega_r}{n\omega_r}\right),\\
&F_n(K_u) = \left[\frac{n\,K_u}{1+\frac{K_u^2}{2}}\right]^2 f_{b,n}^2,\\
&f_{b,n} = J_{\frac{n-1}{2}}(n\xi_u) - J_{\frac{n+1}{2}}(n\xi_u)\ ,\\
&\xi_u = \frac{1}{4}\frac{K_u^2}{1+\frac{K_u^2}{2}}.
\end{aligned} \tag{29}$$

The quantity $F_n(K_u)$ is of crucial importance for the FEL operation on the fundamental and at higher harmonics. It depends on the undulator equivalent strength parameter and therefore on the power density feeding the waveguide, according to the practical formula [10]

$$\begin{aligned}
&B_u[T] \cong b_u[T]f(x), \quad b_u[T] \cong 1.3\cdot 10^{-4}\sqrt{\frac{P[MW]}{S[m^2]}},\\
&f(x) = (1-x^2)^{-\frac{1}{4}} + (1-x^2)^{\frac{1}{4}}, \quad x = \frac{\omega_c}{\omega}, \quad S = ab,\\
&K_u \cong 1.86 b_u[T]a[cm]g(x)f(x), \quad g(x) = \frac{x}{1+\sqrt{1-x^2}}, \quad \lambda_u = 2ag(x).
\end{aligned} \tag{30}$$

It is worth taking into account that a new parameter ($x = \omega_c/\omega$) controlling the tunability of an MU-FEL comes into play. It provides the definition either of equivalent undulator period or strength parameters. The importance of this quantity will be commented on in the following.

The behavior of K_u and of $F_n(K_u)$ vs. the microwave power is provided in Figure 4 which yields an idea of the power necessary to obtain reasonable K_u values for FEL operation, either in the oscillator or in SASE configurations. This quantity is indeed critical to fix the value of the small signal gain coefficient [25,27], representing the reference value for oscillator FEL

$$g_0 = \frac{16\pi}{\gamma}\frac{|J|}{I_0}\lambda_r L N_u^2 \xi_u f_{b,1}^2 \tag{31}$$

with $J = \hat{I}/\Sigma$ the current density, $\hat{I}$ the e-beam peak current and Σ the e-beam cross section.

It is worth underscoring that apart from the obvious (and not secondary) technological details the search for the relevant design and optimization criteria does not change with respect to the strategy developed in the past [29].

In the following, we limit our examples to devices operating in the IR-UV region. In Figure 5a,b, we have plotted the equivalent undulator period length vs. $x = \omega/\omega_c$ and the FEL operating wavelength vs. the beam relativistic factor. It is worth stressing that large

x values shift λ_r towards longer wavelengths. This fact, as we will see in the following, will have consequences on the gain itself.

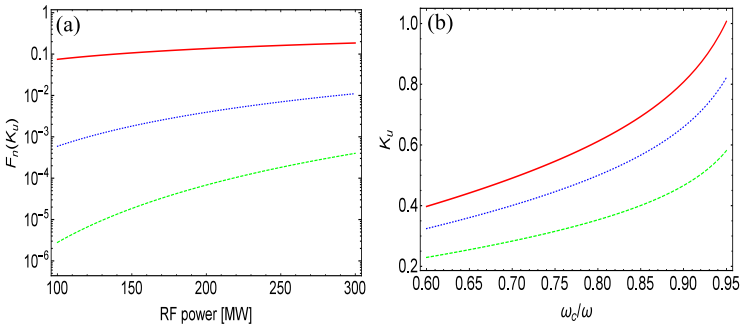

Figure 4. (**a**) $F_n(K_u) = \left[\frac{n\,K_u}{1+\frac{K_u^2}{2}}\right]^2 f_{b,n}^2$ vs. microwave power, n = 1 (solid line), n = 3 (dotted line), n = 5 (dashed line); (**b**) strength parameter K_u vs. $\frac{\omega_c}{\omega}$ for different values of the microwave power, 300 MW (solid), 200 MW (dotted), 100 MW (dashed).

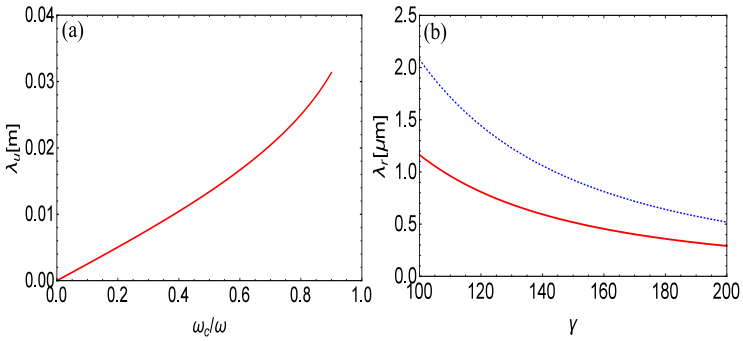

Figure 5. (**a**) Equivalent undulator period vs. $x = \omega_c/\omega$; (**b**) resonant wavelength vs. γ (dot $x = 0.9$, continuous $x = 1/\sqrt{2}$).

In Figure 6a–c, we have reported the behavior of g_0 in terms of the microwave parameters. In particular, in Figure 6a we have plotted the small signal gain coefficient vs. the microwave power for a FEL operating in the sub-micron region for two different beam energies (50 and 100 MeV) and 120 A peak current. In Figure 6b, we have reported the gain coefficient vs. the resonant wavelength.

The values of g_0 we have evaluated with the parameters listed in Figure 6 confirm the possibility of operating an MU-FEL oscillator driven by a low energy Linac with good beam characteristics (see next section, for the necessary details) in the region ranging from near IR to UV. The operation with larger x values is favored because it ensures larger values of the strength parameter (see Figure 4b) (which remains limited to values not exceeding 0.4). The wave undulator period vs. $\frac{\omega}{\omega_c}$ is shown in Figure 5a. For example, in correspondence of $\omega = \frac{\omega_c}{\sqrt{2}}$, we find $\lambda = 2$ cm, which yields reasonable K values and the possibility of a compact device. Even though the architecture of an FEL oscillator device is fairly simple, further details for the necessary implementation should be specified. In particular, we need to examine the problem of the focusing, namely the necessity of including additional quadrupoles ensuring the proper electron transport (see Appendix A).

Let us now consider a specific set of parameters for a microwave undulator FEL oscillator operating in the sub-micron region with the parameters reported below (wave guide dimensions and power a[cm] = 2.5, b[cm] = 1.25, P[MW] = 100).

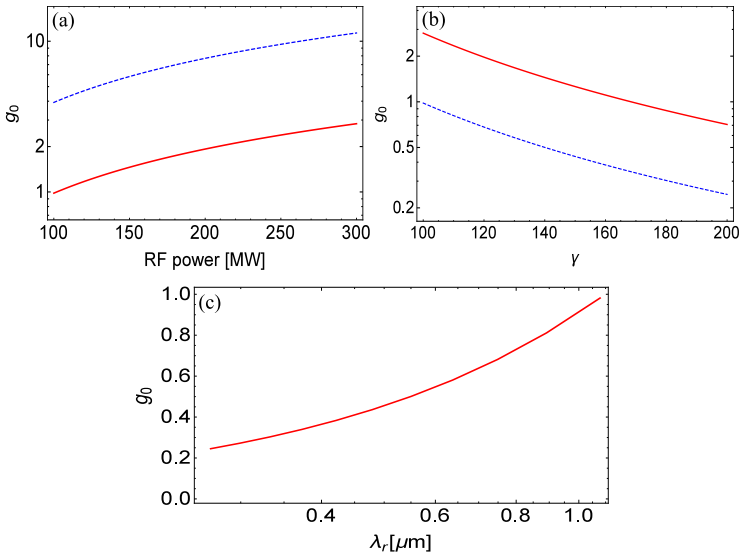

Figure 6. (**a**) g_0 vs. microwave power (MW) for different values of the beam energy (dash 50 MeV, continuous 100 MeV) $x = \frac{1}{\sqrt{2}}$; (**b**) g_0 vs. the beam energy for different values of the microwave power (dashed line 100 MW, solid line 300 MW); (**c**) g_0 vs. FEL resonant wavelength ($x = 1/\sqrt{2}$ and $P = 100$ MW), for the remaining parameters see Table 1.

Table 1. Sub-micron MU-FEL oscillator design parameters.

Beam Current [A]	120
Beam Energy [MeV]	60
Normalized Beam emittance [mm·mrad]	5
Twiss Parameter β [m]	5
Beam Relative Energy spread (σ_ε)	0.1%
Microwave Power [MW]	100
Equivalent undulator Period length λ_u [cm]	2
Undulator parameter Strength	$K_u = 0.277$
FEL operating wavelength	$\lambda \cong 0.7$ μm
Number of Undulator Periods	100

The small signal gain coefficient evaluated with the previously listed parameters is larger than 30%, and in absence of any inhomogeneous broadening detrimental effect (see the next section), we find the maximum gain [30] $G \cong 0.85 g_0 + 0.19 g_0^2 \cong 29\%$.

We have assumed a relative energy spread of the order of 0.1% to avoid significant gain reduction due to line inhomogeneous broadening. The amount of gain detrimental effect according to the parameters listed in Table 1 is a reduction factor $R = 0.786$, which is not particularly harmful (for further comments see below). This small energy spread requires particular care in the choice of the Linac, which can be, e.g., super conducting.

The operation with an oscillator requires a low losses cavity where the round-trip intra-cavity signal grows as indicated in Figure 7 , where we have exploited the following relationships

$$I_{r+1} = I_0 \frac{[(1-\eta)\ (G_M+1)]^{\,r}}{1+\frac{I_0}{I_e}\{\,[(1-\eta)\ (G_M+1)]^{\,r}-1\}},$$

$$I_e = \left(\sqrt{2}+1\right)\left(\sqrt{\frac{1-\eta}{\eta}G_M}-1\right)I_S, \tag{32}$$

$$I_s \equiv I_S\left[\frac{MW}{cm^2}\right] = 6.9312\cdot 10^2 \frac{1}{2}\left(\frac{\gamma}{N}\right)^4 (\lambda_u[cm]\,K^* f_b)^{-2} \equiv \text{saturation intensity},$$

where r is the round-trip number, I_0 is the seed signal, and η is the cavity losses.

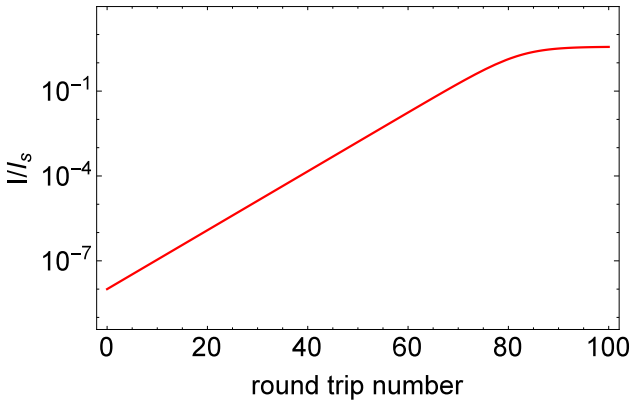

Figure 7. Normalized intracavity laser intensity ($X = I/I_s$) vs. the round-trip period. For an oscillator operating with the parameters of Table 1 and with total losses $\eta \cong 5\%$.

The use of a cavity with a length of 2.5 m ensures the saturation in a time provided by

$$\tau^*[s] \cong 6.7\cdot 10^{-9}\frac{\ln(0.1\,I_e/I_0)}{\ln[(1-\eta)\ G_M+1]}L_c[m], \tag{33}$$

not exceeding 1.5 μs. Furthermore, for a properly optimized cavity [30], the saturated output peak power($P_L \cong 1/4N\cdot P_E$) is 18 MW. The average power depends on the characteristics of the RF accelerating field and will not be discussed in the present context.

It is evident that the example we have presented is just aimed at underscoring that the operation of a FEL oscillator is possible. The use of less relaxed parameters (even though not far from the present technological capabilities), see Table 2, indicates the possibility of extending the operation to the UV region.

The evaluated value of g_0 at the UV region is shown in Figure 8.

The analysis we have developed so far is incomplete because we have limited the discussion to the low gain regime, and we did not include beam and undulator characteristics which determine, through inhomogeneous broadening, gain degrading effects [30].

In the forthcoming section, we complete the analysis by including these detrimental contributions and discuss the possibility of an X-ray MU SASE-FEL operation.

Table 2. Same as Table 1 for the UV operation. Regarding the relative energy spread, we have assumed a linear scaling with the inverse of the energy. Therefore, with respect to the case of Table 1, we foresee $\sigma_\varepsilon = 5 \times 10^{-4}$.

Beam Current [A]	120
Beam Energy [MeV]	100
Normalized Beam emittance [mm·mrad]	10
Twiss Parameter β [m]	5
Equivalent undulator Period length λ_u [cm]	0.77–1.3
Undulator parameter Strength	$K_u = 0.15$–0.26
FEL operating wavelength	$\lambda \cong$ 100–170 nm
Number of Undulator Periods	200
Microwave Power [MW]	200

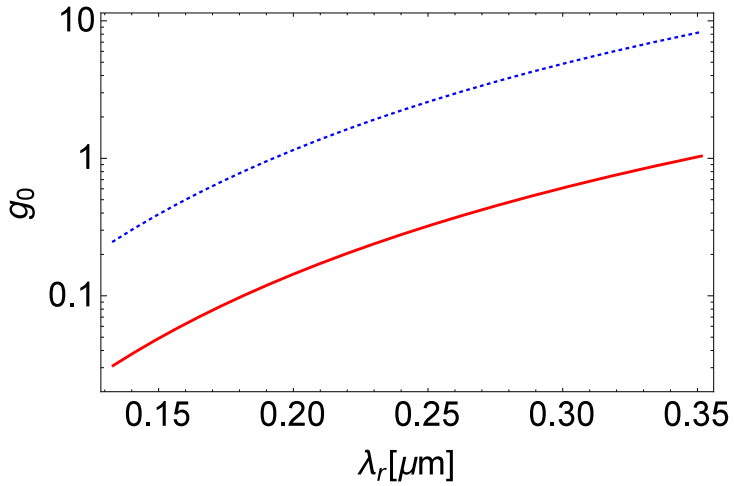

Figure 8. Small signal gain coefficient vs. resonant wavelength for values of *RF Power* = 200 MW, $\gamma = 200$ and $N_u = 100$ (continuous line) and $N_u = 200$ (dotted).

4. Sources of Inhomogeneous Broadening and High Gain Regime

It is well-known that any deviation from the ideal conditions, either in the undulator field or in the electron beam qualities, induces elements of gain deterioration, which may create a drawback to the FEL performance. These effects are known as inhomogeneous broadening contributions [29–33]. This last term indicates the deviation from the "natural" line width $\left(\left(\frac{\Delta\lambda}{\lambda}\right)_0 = \frac{1}{2N_u}\right)$ and determines a line broadening with a consequent gain reduction. The impact of these effects can be quantified through the use of the so-called inhomogeneous broadening coefficients.

It should be noted that in the case of the magnetic undulator, the sources of field non-homogeneity are due to the transverse MU field components.

The origin of these effects, in the case of waveguide modes, are essentially the same, even though the relevant derivation is trickier.

The line broadening we have mentioned can be easily calculated from the shift in resonant wavelength($\lambda_r = \frac{\lambda_u}{2\gamma^2}\left(1 + \frac{K_u^2}{2} + \gamma^2\vartheta^2\right)$) determined by the deviation from the nominal value of the various quantities specifying λ_r. The wavelength relative shift due to e-beam energy deviation is given by $\frac{\delta\lambda}{\lambda} \cong 2\frac{\delta\gamma}{\gamma}$, which after averaging over the energy distribution (assumed to be Gaussian) yields the following dependence on the root mean

square relative energy spread ($\left\langle \frac{\delta\lambda}{\lambda} \right\rangle \cong 2\sigma_\varepsilon$). The inhomogeneous broadening parameter specifying the amount of gain degradation is provided by the ratio

$$\mu_\varepsilon = \frac{\left\langle \frac{\delta\lambda}{\lambda} \right\rangle}{\left(\frac{\Delta\lambda}{\lambda}\right)_0} = 4N_u\sigma_\varepsilon. \tag{34}$$

The corresponding gain reduction factor is $R = 1/(1 + 1.7\mu_\varepsilon^2)$, and accordingly to be on the safe side, the following condition should be satisfied

$$\mu_\varepsilon << 1 \Rightarrow \sigma_\varepsilon << \frac{1}{4N_u}, \tag{35}$$

which becomes rather difficult to be satisfied if large equivalent periods are to be chosen. In the case of $N_u \geq 100$, the MU-FEL oscillator becomes rather problematic, because of the extremely good energy quality required for a low energy Linac. The choice of N_u is therefore a matter of a careful optimization of the MU-FEL design and, possibly, some trade-offs.

The next quantity is the equivalent undulator strength, whose deviations from nominal values comes into play from the shifts associated with the equivalent magnetic field and period ($B_u$and λ_u). We find, accordingly, that

$$\frac{\Delta K_u}{K_u} = \frac{\Delta B_u}{B_u} + \frac{\Delta\lambda_u}{\lambda_u}, \tag{36}$$

and therefore the deviation from the ideal conditions comes from technological and physical constraints.

Let us discuss the two contributions separately. We consider first the deviations associated with B_u and find

$$\frac{\Delta B_u}{B_u} = \frac{\Delta E_0}{E_0} + \frac{\Delta\left(\sqrt{1-\left(\frac{\omega_c}{\omega}\right)^2}\right)}{1+\sqrt{1-\left(\frac{\omega_c}{\omega}\right)^2}} = \frac{\Delta E_0}{E_0} + \frac{x\left|\left(\frac{\Delta a}{a} + \left(\frac{\Delta\lambda}{\lambda}\right)_c\right)\right|}{1+\sqrt{1-x^2}},$$
$$\left(\frac{\Delta\lambda}{\lambda}\right)_c \equiv \text{microwave line} - \text{width}. \tag{37}$$

The electric field deviation from the nominal value is specified in terms of the power density waveguide fluctuation

$$E_0 \cong \sqrt{\frac{Z_0 P}{ab}},$$
$$Z_0 = 120\pi\,\Omega \equiv vacuum - impedance. \tag{38}$$

Including the other term, due to the waveguide size and line width, we can write the first term in Equation (36) as reported in ref. [10]

$$\frac{\Delta B_u}{B_u} \cong \left[\frac{1}{2}\frac{\Delta P}{P} + 0.59\left|\frac{\Delta a}{a}\right| + 0.5\left|\frac{\Delta b}{b}\right| + 9\cdot 10^{-2}\left(\frac{\Delta\lambda}{\lambda}\right)_c\right]. \tag{39}$$

Finally, regarding the equivalent undulator period shift, we have [10]

$$\frac{\Delta\lambda_u}{\lambda_u} \cong \left[\sqrt{2}\left(\frac{\Delta\lambda}{\lambda}\right)_c + \left(\sqrt{2}-1\right)\left|\frac{\Delta a}{a}\right|\right]. \tag{40}$$

Before defining the parameters, it is necessary to quantify the effects associated with the gain dilution. We remember that the FEL line shift due to $\Delta K_u/K_u$ is [31]

$$\left(\frac{\delta\omega}{\omega}\right)_{K_u} \cong \left| \frac{K_u^2}{1+\frac{K_u^2}{2}} \left[\frac{\Delta B_u}{B_u} + \frac{\Delta\lambda_u}{\lambda_u}\right] \right| \cong \frac{K_u^2}{1+\frac{K_u^2}{2}} \left[\frac{\Delta P}{2P} + \sqrt{2}\frac{\Delta a}{a} + \sqrt{2}\left(\frac{\Delta\lambda}{\lambda}\right)_c\right], \tag{41}$$

with $\Delta a/a \approx \Delta b/b$.

These line shifts can in principle be treated as sources of inhomogeneous broadening, provided that they are statistically independent in such a way that the induced root mean square line width can be defined as

$$\left(\frac{\delta\omega}{\omega}\right)_{K_u,rms} = \sqrt{\left\langle \left(\frac{\delta\omega}{\omega}\right)^2_{Ku} \right\rangle - \left\langle \left(\frac{\delta\omega}{\omega}\right)_{Ku} \right\rangle^2}, \tag{42}$$

where the averages are taken on the distributions associated with the power fluctuation distributions, with the transverse dimension waveguide uncertainties and spectral width. In order to define a useful reference quantity, we proceed as for the case of the energy spread and introduce the quantity

$$\begin{aligned} \mu_{K_u} &= 2N_u \left(\frac{\delta\omega}{\omega}\right)_{K_u,rms} \cong N_u\xi\sqrt{\sigma_p^2 + 8\sigma_a^2 + 8\sigma_c^2}, \\ \sigma_p &= \left\langle \frac{\Delta P}{P} \right\rangle_{rms}, \\ \sigma_a &= \left\langle \frac{\Delta a}{a} \right\rangle_{rms}, \\ \sigma_c &= \left\langle \left(\frac{\Delta\lambda}{\lambda}\right)_c \right\rangle_{rms}. \end{aligned} \tag{43}$$

The importance of these parameters is easily inferred if we take into account that the RF power can be controlled to 10^{-4} and the mechanical errors affecting the cavity dimensions to 10^{-3}, while $\left(\frac{\Delta\lambda}{\lambda}\right)_c$ does not contribute since the associated deviation are better than 10^{-8}. For the low gain regime, these effects are not fully negligible, and the most significant contributions come from the inhomogeneous broadening due to cavity dimension shift machining errors.

A further comment regarding the analysis of the gain depressing terms should be added. We have treated them as inhomogeneous broadenings as a consequence of the assumption that they are associated with independent statistical distributions, which determine the quantification of the amount of their effect through the previously defined μ_{K_u} parameters. This is true regarding the variation of the waveguide transverse size. It reflects as a variation of the transverse $TE_{0,1}$ mode distribution not dissimilar from the dependence of the magnetic field of ordinary undulators on the transverse coordinates. Regarding the waveguide power fluctuations or variations, the assumption is only partially true, as further discussed in the concluding section.

Analogous considerations hold for the high gain regime. The pivotal parameter for this operation is the so called Pierce parameter [25,27], which in practical units is written as

$$\rho \cong \frac{8.36\cdot 10^{-3}}{\gamma}\left[J\left[\frac{A}{m^2}\right]\lambda_u[cm](K_u f_b)^2\right]^{\frac{1}{3}}. \tag{44}$$

It fixes either the gain length ($L_g = \frac{\lambda_u}{4\pi\sqrt{3}\rho}$), the saturated power or the importance of the inhomogeneous broadening gain deterioration effects. We limit ourselves to the soft X-ray operation, and the "design" parameters are given in Table 3.

In Figure 9, we have plotted the achievable values of the Pierce parameter for an SASE MU-FEL operation and the associated gain length (see Table 3 for the parameters used in the calculations).

The parameter case we have considered is not dissimilar to those of ref. [11] (see also Figure 10), and concerning the FEL output performances, the conclusions are that in the case of short wavelength SASE FELs, the MU offers, in principle, some advantages. The most noticeable of them is the short period, hence the possibility of operating with lower e-beam energie, and reducing the overall size and cost of the device. Furthermore, the larger transverse size, not limited by the gap of the conventional undulator magnets, reduces the wake field effects, thus allowing the use of higher currents.

Table 3. Soft X-ray SASE MU-FEL operation.

Beam Current [A]	1500
Beam Energy [MeV]	1300
Normalized Beam emittance [mm·mrad]	1
Twiss Parameter β [m]	5
Microwave Power [MW]	200
Equivalent undulator Period length λ_u [cm]	0.77–1.8
Undulator parameter Strength	$K_u = 0.15$–0.35
FEL operating wavelength	$\lambda \cong$ 2–5 nm

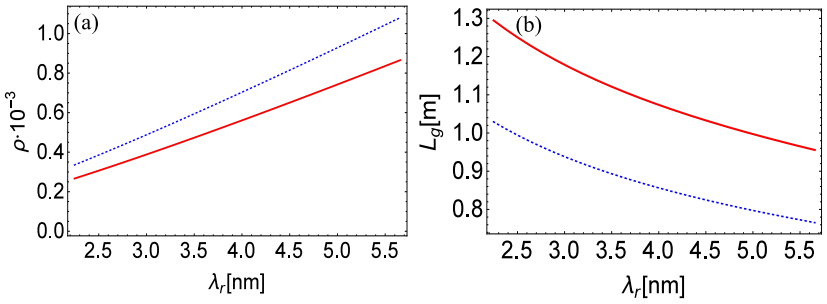

Figure 9. (**a**) Pierce parameter vs. wavelength (**b**) gain-length vs. wavelength $P = 200$ MW (solid line) $P = 400$ MW (dotted line).

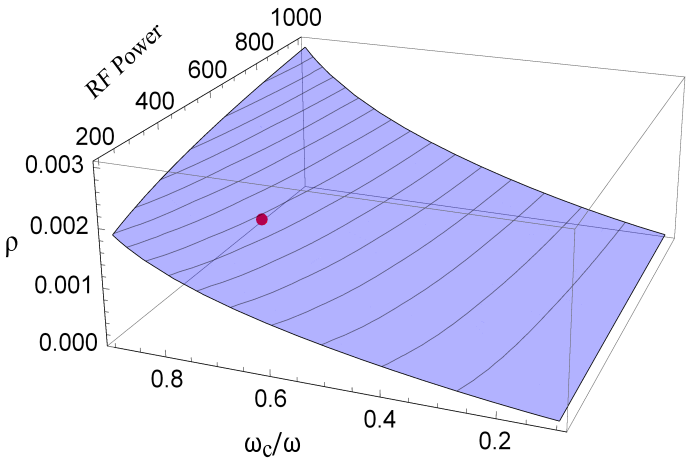

Figure 10. Pierce parameter vs. RF power. The dot indicates the working point of ref. [11].

To make the comparison more fair, we should, however, mention that in the region above 1.5 and 1.8 cm period length, magnetic undulator of superconducting type could be exploited. The relevant performances could be comparable (if not better) than those of MU-FEL s.

Shorter magnetic undulator periods become more problematic even for the super conducting option. The MU solution for a shorter period is also not easily viable, either for the large intra-waveguide power involved or for the technological problems mentioned below.

We must, however, emphasize that the achievable values of the Pierce parameter are below the threshold of 10^{-3}, a circumstance which imposes extremely demanding beam performances in terms of, e.g., energy spread. The condition to be satisfied is that $\sigma_\varepsilon < 2/\rho$ [30,34,35]. Regarding the present paper, an energy spread better than 10^{-4} should be taken into account (ref. [11] considers 6.5×10^{-5}). By applying the rule of thumb, we can conclude that the saturation length is about $20L_g$ without the energy spread effects. The relevant inclusion determines an increase by a factor

$$\begin{aligned} R &= (1 + d\tilde{\mu}_\varepsilon^2), \\ \tilde{\mu}_\varepsilon &= \frac{2\sigma_\varepsilon}{\rho}, \quad d \cong 0.187\frac{\sqrt{3}}{2}. \end{aligned} \tag{45}$$

It is evident that larger values of the MU power could in principle provide better performance, but circulating power larger than 200 MW imposes the use of very high-performing waveguides with extremely large Q-values and low losses. The bottleneck of an MU-FEL device is associated with all evidence to the intrinsic low K values due either to the short period or maximum microwave achievable power (see Equations (2) and (3)). This determines lower gain than ordinary FELs operating with permanent magnet undulators. Therefore, the MU remains of interest for FEL frequencies not exceeding those of soft X-ray.

The problems associated with the beam qualities do not represent the most significant part of the problem. The inhomogeneous problems associated with the power fluctuations, which are controlled within 10^{-4}, are a considerable source of gain degradation. Even worse are the mechanical tolerances which if within 10^{-3} are the most significant technological problems to be solved.

5. Final Comments

In this article, we have discussed how the general criteria for the design of an MU-FEL can be evaluated. In particular, we have included in the FEL scaling design the parameters regarding the MU performance. As already emphasized, any quantity associated with the waveguide design may be a source of troubles for the FEL performance.

Regarding the control of the power inside the waveguide, it should be noted that along with the power fluctuations $\frac{\Delta P}{P}$ discussed in the previous section, another problem is associated with the power losses in the waveguide walls. This is reflected in a reduction of the equivalent undulator strength parameter value, thus leading to a reduction of the resonant wavelength. Large changes in power may hamper the FEL operation. In order to quantify the importance of these effects, we note that the decrease of the strength parameter K along the longitudinal direction z is [11,20]

$$K_u(z) = K_u^0 e^{-\beta_{att} z}, \tag{46}$$

where β_{att} is the attenuation coefficient (AC).

The wavelength reduction associated with a non-zero (but sufficiently small) AC is provided by

$$\left| \frac{\Delta\lambda}{\lambda} \cong \beta_{att}\Delta z \right|. \tag{47}$$

In order to avoid any harmful effect, this shift should be well contained within the SASE gain line width, keeping $\Delta z = L_g$. According to Equation (47) this requires

$$\beta_{att} L_g < \rho, \tag{48}$$

namely

$$\beta_{att} < 4\pi\sqrt{3}\frac{\rho^2}{\lambda_u}. \tag{49}$$

The effects associated with Ohmic power losses cannot be treated as a non-homogeneous broadening. It is not due to statistical effect but to the continuous variation of the decay of the waveguide power, determining the behavior reported in Equation (46).

The effect of such a "deterministic" variation of the magnetic field can be included in the high-gain FEL integral equation [30]

$$\partial_\tau a = \imath\pi g_0 \int_0^\tau \xi e^{-\imath\nu\xi + \frac{\imath\pi\mu_T}{2}\xi(2\tau-\xi)} a(\tau-\xi)d\xi, \tag{50}$$

where

$$\mu_T = 2N\frac{\Delta B}{B}\frac{K_0^2}{1+\frac{K_0^2}{2}}, \qquad \delta B = B(L_u) - B(0). \tag{51}$$

where ΔB is the variation of the equivalent undulator field in one section of length L_u. The possibility of counteracting this effect is tapering the waveguide transverse area in order to increase the power density and therefore the associated K_u values. The amount of tapering can be quantified using Equation (49), which, using typical high gain parameter, yields $\frac{\Delta a}{a} \ll 10^{-2}$, consistent with analogous conclusions reported in ref. [10].

In our previous considerations, we have not included the effects due to the electron beam divergence, which is the source of further gain degradation effects. They are not significant for the values of emittance we have considere, but can become important if we consider the angular spread induced by the width variation of the waveguide transverse dimensions. Rewriting the results of ref. [10] using our formalism and approximation, we find

$$\langle x' \rangle \cong \frac{K_u}{\gamma}\frac{k_u}{\sqrt{k_u^2 + l_c^{-2}}}\sqrt{\frac{N_u\lambda_u}{l_c}}\sigma_a, \tag{52}$$

where l_c is the characteristic coherence length of the statistical process governing the randomness of cavity thickness variations (for further comments see ref. [10]).

The inhomogeneous broadening parameter characterizing the effect of the gain degradation is

$$\mu' \cong \frac{1}{\rho}\left[\frac{K_u}{1+\frac{K_u^2}{2}}\frac{k_u}{\sqrt{k_u^2 + l_c^{-2}}}\sqrt{\frac{N_u\lambda_u}{l_c}}\sigma_a\right]^2, \tag{53}$$

and the use of $l_c \cong 0.1$ mm, $\sigma_a \cong 10^{-3}$, $\lambda_u = 2$ cm, $N_u\lambda_u \cong 7$ cm, $\rho \cong 10^{-3}$ yields an apparently not harmful contribution. By keeping less optimistic parameters ($l_c \cong 0.005$ mm, $\sigma_a \cong 10^{-2}$), the associated gain degradation is not insignificant.

The process leading to the root mean square angular spread in Equation (52) is diffusive (it depends on the square root of the traveled distance); it also determines an increase of the beam transverse size and eventually of the emittance, which should be carefully adjusted by the use of correcting coils or additional focusing elements.

We should furthermore add a few remarks on the role played by the e-beam transport in the waveguide in the design of MU-FEL devices. We have based our analysis on the possibility of reducing the waveguide field to a static equivalent counterpart, and we have introduced the associated period and strength parameter. We have also noted that the motion along the y direction is "naturally" focused, and the relevant equation accounting for the y-slow motion along the waveguide axis is

$$\begin{aligned} &\ddot{y}_s = -k_\beta^2 y_s, \\ &k_\beta = \frac{\pi K_u}{\lambda_u \gamma} \equiv \text{betatron motion wave number.} \end{aligned} \tag{54}$$

Accordingly, the "natural" β Twiss parameter associated with k_β in Equation (54) is

$$\beta_y = k_\beta^{-1} = \frac{\lambda_u \gamma}{\pi K_u}. \tag{55}$$

In Figure 11, we reported the plot of β_y vs. RF power using the same parameters of ref. [11]. The plot shows that the natural focusing is not sufficient to reach the required values of β, ensuring sufficient current density to reach reasonable gain length. Additional quadrupoles are therefore necessary, either to focus the beam in the x-direction or to compensate the weak focusing of β_y.

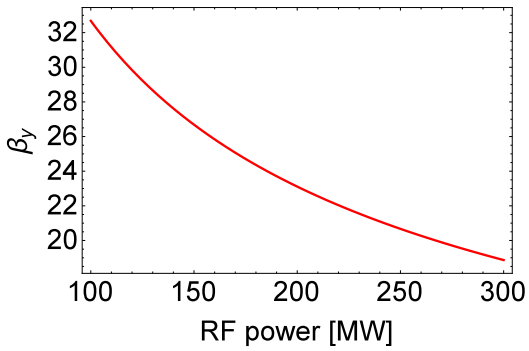

Figure 11. Twiss parameter β_y vs. RF power for $E = 0.7$ GeV, $a = b = 1.8$ cm, $x = 1/\sqrt{2}$.

In this paper, we have discussed the general criteria for the study of an MU-FEL. The presented analysis leads us to the the conclusion that FEL-based MUs are both feasible and promising. Therefore, the problems associated with their realization are not of fundamental nature, but ratherare associated with technical issues, e.g., the control of power fluctuation, very low losses waveguide and high mechanical tolerances of the cavity wall machining.

A possible solution to operate with a low attenuation waveguide is the use of a resonant-ring cavity [10], where the high circulating power is ensured by the low attenuation coefficient. It can in turn be obtained by an adequate choice of the surface material and operating conditions (normal/supeconducting). Regarding the normal conducting option, the use of copper may be a good solution, since at room temperature the copper resistance is low [10]. The super-conducting option is within this respect significantly more advantageous [9,10], but makes the device more difficult and more expensive to build and operate. We hope that an acceleration of the research on these topics will eventually lead to the realization of the potential of MU in the next generation of advanced FELs.

It is evident that we have presented examples based on borderline technologies underlying the use of MU for FEL operation. We have emphasized that significant efforts are necessary to overcome the challenges associated with the MU, and we mentioned how these reflect on the request on the e-beam qualities. We have assumed high brightness e-beams (in particular high-current Linacs with hardly achievable small energy spread).

Furthermore we have pushed on the required waveguide power necessary to reach useful strength parameters for the FEL operation. In conclusion, we can state that the MU option for FEL operation is certainly interesting but imposes severe R&D technological efforts involving a non-straightforward impact on the design strategies for the associated e-beam drivers.

The inclusion of the design concept for this type of LINAC goes beyond the purposes of the paper aimed at clarifying what is needed (in terms of current and electron beam qualities) to operate an MU-based FEL.

Author Contributions: The E.D.P., S.S., G.D. made the same contributions in terms of conceptualization, writing, data control and critical reading. All authors have read and agreed to the published version of the manuscript.

Funding: This research received no external funding.

Institutional Review Board Statement: Not applicable.

Informed Consent Statement: Not applicable.

Data Availability Statement: Not applicable.

Acknowledgments: The authors like to thanks Andrea Doria for a fruitful and interesting discussion on the Hamiltonian of the e-beam transport in a RF cavity.

Conflicts of Interest: The authors declare no conflict of interest.

Appendix A

In this article we have just mentioned two points

(a) The "inverse" of the Fermi-Weiszacker-Williams (FWW) [36–38] approximation, which allowed us to treat the field inside the waveguide as a static field.
(b) The focusing effects of the wave undulator on the electron beam.

We underscored, in the introductory section, that Madey [21] used FWW to regard the undulator static field, "seen" by the electrons, as an ensemble of virtual photons. Later on, A. Renieri and one of the authors of this articles (GD) pointed out that the undulator pseudo photon are characterized by a mass, linked to the undulator period by [24]

$$m_\gamma = \frac{\hbar}{\lambda\!\!\!^{-}_u c}, \qquad \lambda\!\!\!^{-}_u = \frac{\lambda_u}{2\pi} \tag{A1}$$

The interpretation of the photons associated with the e-m field inside a waveguideas massive is also well known. In this case the mass size is fixed by the wave cutoff frequency, namely [39,40]

$$m_\gamma = \frac{\hbar}{\lambda\!\!\!^{-}_c c}. \tag{A2}$$

where $\lambda_c = a/2$, if we limit ourselves to the lowest order mode.

The above statement is easily understood, if we note that the waveguide field for TE_{mn} mode can be derived from the vector potential

$$\begin{aligned}
&\vec{A} \equiv (A_x, A_y, 0),\\
&A_x = \frac{1}{\omega} E_0 \sin\left(k_y y\right) \cos(k_x x) \sin(\phi),\\
&A_y = \frac{1}{\omega} E_0 \sin(k_x x) \cos\left(k_y y\right) \sin(\phi),\\
&\phi = \omega t + k_z z + \phi_0,\\
&k_x = \frac{m\pi}{b},\\
&k_y = \frac{n\pi}{a},
\end{aligned} \tag{A3}$$

and that each component of $\vec{A}$ satisfies the Klein-Gordon type equation

$$\left(\frac{1}{c^2}\frac{\partial^2}{\partial t^2} - \frac{\partial^2}{\partial z^2} + \mu^2\right) A_{x,y} = 0, \tag{A4}$$

with ϕ_0 the starting phase and $\mu = m_\gamma c/\hbar$.

The previous considerations underscore that the origin of the approximations, either that due to Madey [21] (revised in [24], as well) or that discussed in this article, can be framed within the same context. However a more conventional application of the method of virtual quanta to treat scattering problems, should deal with the virtual quanta associated with the moving charged particles [36–38]. This procedure, based on the virtual field dressing the electron, while propagating inside a magnetic or wave undulator, has been discussed in refs. [41,42].

A more subtle argument regarding the two approximations, should be raised. The field in Equation (A3) satisfies the Coulomb Gauge condition $\vec{\nabla} \cdot \vec{A} = 0$, while regarding it as static, namely as that of a linearly polarized undulator along the y-direction (see Equation (18)), the corresponding vector field should be derived using the symmetric gauge, namely

$$\vec{A} = -\frac{1}{2}\vec{r} \times \vec{B} \equiv -\frac{E_0}{2c} \sin(k_u z)(-z, 0, x). \tag{A5}$$

The problem is however hampered from the very beginning, since the magnetic field in Equation (18) satisfies the Maxwell equations in a region limited to the magnetic axis. The correcting terms, containing the dependence of the field on the transverse coordinates (see [43,44]), restore the correct field form and justifies the focusing undulator contribution described by Equation (54).

We can however treat the focusing due to the waveguidefield, without any "static" approximation.

We follow the standard procedure, described in e.g., ref. [45], to derive the Hamiltonian characterizing the betatron motion inside the waveguide, which, using the field potentials reported in Equation (A3), can be written as

$$\begin{aligned}
&H = \frac{\delta}{\beta_0} - \sqrt{\left(\frac{1}{\beta_0} + \delta\right)^2 - p_x^2 - p_y^2 - \frac{1}{\beta_0^2\gamma_0^2}} - \frac{1}{\omega}\frac{q}{P_0} E_0 \sin(k_y y) \sin(\psi),\\
&\psi = \frac{ks}{\beta_0} - (k - k_z)z + \phi_0,
\end{aligned} \tag{A6}$$

being $p_{x,y}$ the transverse canonical momentum normalized to the reference momentum P_0, and the longitudinal dynamical variables (z, δ) defined below

$$\left(z = s/\beta_0 - ct, \delta = \frac{E}{P_0 c} - \frac{1}{\beta_0}\right). \tag{A7}$$

To eliminate the explicit dependence of the Hamiltonian on the variable s we make an average along the cavity length $L = \pi/k$

$$\widetilde{H} =< H >= \frac{1}{L}\int_{-L/2}^{L/2} H ds, \tag{A8}$$

and operating a paraxial approximation we eventually end up with

$$\begin{aligned} \widetilde{H} &= \frac{p_x^2}{2} + \frac{p_y^2}{2} + \frac{\delta^2}{2\beta_0^2\gamma_0^2} - K\sin(k_y y)\cos(\phi_0 - (k - k_z)z), \\ K &= \frac{1}{\omega}\frac{2\beta_0}{\pi}\frac{q}{P_0}E_0 \sin\left(\frac{\pi}{2\beta_0}\right). \end{aligned} \tag{A9}$$

The effect of the transverse particle focusing is provided in Figure A1, where the dynamics in the the phase space (y, p_y) is reported.

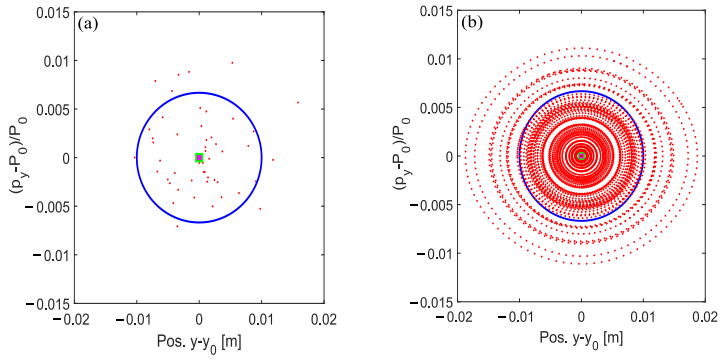

Figure A1. (**a**) Initial particle distribution in y-direction with $\sigma_y = 5 \cdot 10^{-3} m$, $\sigma_{vy} = 1 \cdot 10^6 m/s$, y_0 half the waveguide dimension in the y-direction and P_0 evaluated for $v_x = v_y = 5.6 \cdot 10^6$, $v_z = 2.995 \cdot 10^8$; the blue line is an ellipse centered at (y_0, P_0) with radius 2σ in both the directions. (**b**) The evolution of the distribution in (**a**) governed by the Hamiltonian Equation (A9) for $K = 0.0105$ and a constant phase such that $\cos(\phi_0 - (k - k_z)z_0) = 0.01$.

In a forthcoming dedicated paper we will treat the point (b) without any simplifying assumption. We will indeed use the full relativistic treatment and field potential equations to discuss how the particle phase space problem (and hence focusing) should properly be treated.

References

1. Yulpatov, V.K. Nonlinear theory of the interaction between a periodic electron beam and an electromagnetic wave. *Radiophys. Quantum Electron.* **1967**, *10*, 846–856. [CrossRef]
2. Gaponov, A.V.; Petelin, M.I.; Yulpatov, V.K. The induced radiation of excited classical oscillators and its use in high-frequency electronics. *Radiophys. Quantum Electron.* **1967**, *10*, 794–813. [CrossRef]
3. Ginzburg, N.S. Nonlinear theory of electromagnetic wave generation and amplification based on the anomolous Doppler effect. *Radiophys. Quantum Electron.* **1979**, *22*, 323–330. [CrossRef]
4. Bratman, V.L.; Ginzburg, N.S.; Nusinovich, G.S.; Petelin, M.I.; Strelkov, P.S. Relativistic gyrotrons and cyclotron autoresonance maser. *Int. J. Electron.* **1981**, *13*, 541–567. [CrossRef]
5. Shintake, T.; Huke, K.; Tanaka, J.; Sato, I.; Kumabe, I. Development of Microwave Undulator. *Jpn. J. Appl. Phys.* **1983**, *22*, 844–851. [CrossRef]

6. Batchelor, K. *Microwave Undulator*; Brookhaven National Laboratory Report: Upton, NY, USA, 1983.
7. Danly, B.; Bekefi, G.; Davidson, R.; Temkin, R.; Tran, T.; Wurtele, J. Principles of Gyrotron Powered, Electromagnetic Wigglers for Free-Electron Lasers. *IEEE J. Quantum Electron.* **1987**, *23*, 103–116. [CrossRef]
8. Tran, T.; Danly, B.; Wurtele, J. Free-Electron Lasers with Electromagnetic Standing Wave Wigglers. *IEEE J. Quantum Electron.* **1987**, *23*, 1578–1589. [CrossRef]
9. Boni,R.; Savoia,A.; Spataro, B.; Tazzioli, F.; Fabbricatore, P.; Parodi, R.; Fernandes, P. Superconducting Microwave Undulator. *Rev. Sci. Instrum.* **1989**, *60*, 1805–1808. [CrossRef]
10. Seidel, M. *Parameter Evaluation for Microwave Undulator Schemes*; report number DESY-TESLA-FEL-2001-08; DESY: Hamburg, Germany, 2001.
11. Pellegrini, C. X-band microwave undulators for short wavelength free-electron lasers. *AIP Conf. Proc.* **2006**, *807*, 30–45.
12. Tantawi, S.; Shumail, M.; Neilson, J.; Bowden,G.; Chang,C.; Hemsing, E.; Dunning, M. Experimental Demonstration of a Tunable Microwave Undulator. *Phys. Rev. Lett.* **2014**, *112*, 164802. [CrossRef]
13. Kuzikov, S.V.; Jiang, Y.; Marshall, T.C.; Sotnikov, G.V.; Hirshfield, J.L. Configurations for short period rf undulators. *Phys. Rev. ST Accel. Beams* **2013**, *16*, 070701. [CrossRef]
14. Savilov, A.V. Compression of complicated rf pulses produced from the super-radiant backward-wave oscillator. *Appl. Phys. Lett.* **2010**, *97*, 093501. [CrossRef]
15. Kuzikov, S.V.; Savilov, A.V.; Vikharev, A.A. Flying radio frequency undulator. *Appl. Phys. Lett.* **2014**, *105*, 033504. [CrossRef]
16. Gaponov, A.V.; Miller, M.A. Potential Wells for Charged Particles in a High-Frequency Electromagnetic Field. *JEPT* **1958**, *7*, 168.
17. Bandurkin, I.V.; Kuzikov, S.V.; Savilov, A.V. Cyclotron-undulator cooling of a free-electron-laser beam. *Appl. Phys. Lett.* **2014**, *105*, 073503. [CrossRef]
18. Zhang, L.; He, W.; Clarke, J.; Ronald, K.; Phelps, A.D.R.; Cross, A. Systematic study of a corrugated waveguide as a microwave undulator. *Appl. Sci.* **2019**, *26*, 11–17. [CrossRef]
19. Di Palma, E.; Ceccuzzi, S.; Ravera, G.L.; Sabia, E.; Spassovsky, I.; Dattoli, G. Radio-Frequency Undulators, Cyclotron Auto Resonance Maser and Free Electron Lasers. *Appl. Sci.* **2021**, *11*, 9499. [CrossRef]
20. Jackson, J.D. *Classical Electrodynamics*, 3rd ed.; John Whiley and Sons Inc.: Hoboken, NJ, USA, 1998.
21. Madey, J.M.J. Stimulated emission of bremsstrahlung in a periodic magnetic field. *J. Appl. Phys.* **1971**, *42*, 1906–1913. [CrossRef]
22. Colson, W.B. Classical free electron laser theory. In *Free Electron Laser Handbook*; Colson, W.B., Pellegrini, C., Renieri, A., Eds.; North-Holland Physics: Amsterdam, The Netherlands, 1990; Volume 6, Chaper 5.
23. Colson, W.B. The nonlinear wave equation for higher harmonics in free-electron lasers. *IEEE J. Quantum Electron.* **1981**, *17*, 1417–1427. [CrossRef]
24. Dattoli, G.; Renieri, A. Experimental and theoretical aspects of the free-electron laser. In *Volume IV, Chapter in Laser Handbook*; Stitch, M.L., Ball, M.S., Eds.; North-Holland: Amsterdam, The Netherlands, 1985. [CrossRef]
25. Dattoli, G.; Renieri, A.; Torre, A. *Lectures on the Theory of Free Electron Laser and on Related Topics*; World Scientific: Singapore, 1993. [CrossRef]
26. Schneidmiller, E.; Yurkov, M. Baseline Parameters of the European XFEL. In Proceedings of the 38th International Free-Electron Laser Conference, Santa Fe, NM, USA, 20–25 August 2018; p. MOP033. [CrossRef]
27. Saldin, D.E.; Schneidmiller, E.V.; Yurkov, M.V. *The Physics of Free Electron Lasers*; Springer: Berlin/Heidelberg, Germany, 2000. [CrossRef]
28. Kim, K.-J. Characteristic of Synchrotron Radiation. *AIP Conf. Proc.* **1989**, *184*, 565–632. [CrossRef]
29. Dattoli, G.; Ottaviani, P.L. Semi-analytical models of free electron laser saturation. *Opt. Commun.* **2002**, *204*, 283–297. [CrossRef]
30. Dattoli, G.; Ottaviani, P.L.; Pagnutti, S. Booklet of FEL Design. 2007. Available online: http://fel.enea.it/booklet/pdf/Booklet_for_FEL_design.pdf (accessed on 27 June 2016).
31. Dattoli, G.; Letardi, T.; Madey, J.; Renieri, A. Limits on the single-pass higher harmonics FEL operation. *IEEE J. Quantum Electron.* **1984**, *20*, 1003–1005. [CrossRef]
32. Colson, W.B.; Gallardo, J.C.; Bosco, P.M. Free-electron-laser gain degradation and electron-beam quality. *Phys. Rev. A* **1986**, *34*, 4875–4881. [CrossRef]
33. Dattoli, G.; Renieri, A.; Torre, A.; Caloi, R. Inhomogeneous broadening effects in high-gain free electron laser operation: A simple parametrization. *Il Nuovo Cimento D* **1989**, *11*, 393–404. [CrossRef]
34. Xie, M. Design optimization for an X-ray free electron laser driven by slac linac. *Proc. Part. Accel. Conf.* **1995**, *1*, 183–185. [CrossRef]
35. Dattoli, G.; Giannessi, L.;Ottaviani, P.L.; Ronsivalle, C. Semi-analytical model of self-amplified spontaneous-emission free-electron lasers, including diffraction and pulse-propagation effects. *J. Appl. Phys.* **2004**, *95*, 3206–3210. [CrossRef]
36. Fermi, E. Über die Theorie des Stoßes zwischen Atomen und elektrisch geladenen Teilchen. *Z. Phys.* **1924**, *29*, 315–327. [CrossRef]
37. Weizsäcker, C.F.V. Ausstrahlung bei stößen sehr schneller elektronen. *Prog. Part. Nucl. Phys.* **1934**, *99*, 612–625. [CrossRef]
38. Williams, E.J. Nature of the High Energy Particles of Penetrating Radiation and Status of Ionization and Radiation Formulae. *Phys. Rev.* **1934**, *45*, 729–730. [CrossRef]
39. Wang, Z.-Y.; Xiong, C.-D. Photons inside a waveguide as massive particles. *arXiv* **2007**, arXiv: 0708.3519.
40. Robles, P.; Claro, F. Can there be massive photons? A pedagogical glance at the origin of mass. *Eur. J. Phys.* **2012**, *33*, 1217–1226. [CrossRef]

41. Zolotorev, M.S.; McDonald, K.T. Classical Radiation Processes in the Weizsacker-Williams Approximation. *arXiv* **2000**, arXiv: physics/0003096.
42. Dattoli, G.; Nguyen, F. Free electron laser and fundamental physics. *Prog. Part. Nucl. Phys.* **2018**, *99*, 1–28. [CrossRef]
43. Krinsky, S.; Perlman, M.L.; Watson, R.E. Characteristics of synchrotron radiation and of its sources. In *Handbook of Synchrotron Radiation*; Koch, E.E., Ed.; North-Holland Publishing Company: Amsterdam, The Netherlands, 1983; pp. 65–171.
44. Dattoli, G.; Ottaviani, P.L. Electron beam propagation in linearly polarized undulators: The effect of the anharmonicity on the spatial and phase-space distributions. *J. Appl. Phys.* **1995**, *78*, 1348–1357. [CrossRef]
45. Wolski, A. *Beam Dynamics in High Energy Particle Accelerators*; Imperial College Press: London, UK, 2014.